

Influence of Particle Shape on Filtration Processes

Lucija Boskovic,¹ Igor S. Altman,^{1,2} Igor E. Agranovski,¹ Roger D. Braddock,¹
Toshihiko Myojo,³ and Mansoo Choi²

¹*Faculty of Environmental Sciences, Griffith University, Brisbane, Australia*

²*National CRI Center for Nano Particle Control, Institute of Advanced Machinery and Design, Seoul National University, Seoul, Korea*

³*National Institute of Industrial Health, Nagao, Tama, Kawasaki, Japan*

The influence of particle shape on filtration processes was investigated. Two types of particles, including spherical polystyrene latex (PSL) and iron oxide, and perfect cubes of magnesium oxide, were examined. It was found that the removal efficiency of spherical particles on fibrous filters is very similar for corresponding sizes within the range of 50–300 nm, regardless of the fact that the densities of PSL and iron oxide differ by a factor of five. On the other hand, the removal efficiency of magnesium oxide cubic particles was measured, and found to be much lower than the removal efficiency for the aerodynamically similar spheres. Such disparity was ascribed to the different nature of the motion of the spherical and cubic particles along the fiber surface, following the initial collision. After touching the fiber surface and before coming to rest, the spherical particles could either slide or roll compared to the cubic ones, which could either slide or tumble. During tumbling, the area of contact between the particle and the fiber changes significantly, thus affecting the bounce probability, whilst for the spheres, the area of contact remains the same for any point of the particle trajectory. The extra probability of particle bounce by the cubes was derived from the experimental data. The particle kinetic energy was proposed to be responsible for the difference in removal efficiency of particles with alternative shapes, if all other process parameters remain the same. The increase in kinetic energy is shown to favor the increase of the bounce probability.

INTRODUCTION

Filtration is the most common method of aerosol monitoring and control. The classical filtration theory (see Hinds 1999, for example) does not pay much attention to particle bounce during capture by the filter fiber. However, recent experiments (Mullins, Agranovski, and Braddock 2003) show that particle bounce may significantly change the filter efficiency. A number of theories (Bradley 1932; Hamaker 1937; Johnson, Kendall, and Roberts 1971; Wang and Kasper 1991; Dahneke 1995; Wall et al., 1990)

were developed to describe the particle interaction with the surface of the filter and to estimate the probability of the particle adhesion onto a surface.

A range of particle, filter and process parameters could contribute to the strength of the adhesion. They include hardness (Loeffler 1974) and cross-sectional shape of the fiber (Loeffler 1971), smoothness of either the fiber or particle (Deryaguin et al. 1987), air humidity (Stenhouse 1972), and many others. Obviously, the particle size (and correspondingly the surface area) also plays a crucial role in the bouncing processes. It was found that adhesion forces are greater when acting on bigger size particles. At the same time the air drag force acting on the bigger particles is also larger and this acts so as to detach these larger particles from the fiber at a lower air velocity compared to the smaller ones (Mullins et al. 1992).

Despite its demonstrated importance in filtration research, the detailed mechanisms of the particle-fiber collision and the possibility for the particle to bounce have not been fully investigated. Earlier experimental studies of the collision process have focused on a droplet-surface collision which is quite different from a particle-surface collision (Gillespie and Rideal 1955; Gallily and La Mer 1958). In further experiments conducted by Dahneke (1971, 1973, 1975), a more advanced technique, such as laser Doppler velocimetry, was used to measure the bounce of polystyrene latex (PSL) particles on polished quartz and stainless steel surfaces. Wang and John (1987) and Xu and Willeke (1993) developed techniques involving the impaction of aerosols onto a flat plate to compare bounce properties. The particle deformation during adhesion to a flat surface was examined by Tsai, Pui, and Liu (1991) and Rimai, Demejo, and Bowen (1994). Although this research work was very important for understanding the general principles involved, it is not very useful in understanding the real processes occurring in filtration.

In the cases mentioned above, the surface is massive compared to the particle mass and it behaves as a rigid body. However, where filter fibers are used, they are held in a mat like structure and are able to deform or move as a result of the impact.

Received 15 July 2005; accepted 28 October 2005.

Address correspondence to Igor E. Agranovski, Faculty of Environmental Sciences, Griffith University, Brisbane, 4111 QLD, Australia. E-mail: I.Agranovski@griffith.edu.au

This alters the particle-surface interaction, as the nature of the fiber acts more elastically than a rigid massive surface.

Note that the orientation of the fibers can be random, and that the fiber surface is curved. Thus the point of contact of a particle with a fiber, is on a slanting surface where the particle may or may not adhere; be captured or bounce. Where bounce occurs, the particle may be captured by subsequent collisions with the same fiber or another fiber.

The nature of the particle motion along the fiber surface appears to be important, and collision properties of the particle on the fiber surface depends on the particle shape; as well as on the fiber orientation. Using filters cut from the same material will ensure the same average fiber orientations.

For perfectly spherical particles, the type of motion of the particle in contact with fiber is either sliding or rolling. However, for both forms of the motion of the spherical particle the area of the particle contact with the fiber does not change during the motion. Note that any deformation or elastic “give” in the fiber will increase the time in contact and thus provide greater opportunity for sliding motion to convert to rolling motion. It should be noticed that, even for large spheres, it is difficult to visually distinguish sliding and rolling objects.

A totally different picture would occur in the case of non-spherically shaped particles (cubes, for example), which either slide on a face, or tumble on a corner or edge. During tumbling, the area of the contact changes significantly depending on the form of contact, and may affect the bounce probability, and therefore, the filtration efficiency. If it is the case, some parameter responsible for the contribution of the particle tumbling to the filtration efficiency ought to be introduced.

The particle kinetic energy in the flow was chosen to indicate when the tumbling is significant for the filtration efficiency. As one will see, this parameter should not play any role for the actual filtration of the particles, which could not tumble, as the inertial mechanism for particle removal is negligibly small within the entire range of particle sizes of interest.

The present work is a first step to investigate the dependence of the filter efficiency upon the particle shape from this point of view. In the experiment, we compare the filter efficiency for the polystyrene latex and iron oxide particles that are of spherical shape with cubic magnesium oxide particles of the same equivalent size. The difference found in the efficiency and its dependence on the particle size supports our assumption about the role of tumbling in filtration.

EXPERIMENTAL SET UP AND MEASUREMENT PROCEDURE

Test Aerosol Production

Three various types of nanoparticles were used in this research. They may be classified into two groups: spherical particles with different densities and cubic particles (perfect cubes). The first example of the spherical particles was polystyrene latex with five aerodynamic diameters of 50, 70, 100, 150, and 300 nm supplied by Bangs Laboratories (Fishers, IN, USA). The density of PSL particles is 1.05 g/cm^3 . Spherical iron oxide nanoparticles (density 5.2 g/cm^3) were also used in this project, and these were synthesized by direct metal combustion in an oxygen containing environment (Altman et al. 2004). In brief, pure iron powder was combusted and the nanoparticles from the fumes were collected on a suitable substrate. After collection, particles were gently brushed from the surface and placed in a dry environment. A typical transmission electron microscope (TEM) image of iron oxide particles collected near the generation zone is shown in Figure 1a to demonstrate their sphericity. Dry nanoparticles were added into the nanopure deionized water (resistivity $\rho > 18.0 \text{ M}\Omega$) and sonicated by the ultrasonic bath for 60 minutes to prepare the solution for subsequent aerosolization by a nebulizer. To ensure the looseness of the particles after sonication, the TEM grid was submerged into the suspension to take a sample for following observation through the microscope. The TEM photograph of the sample (see Figure 1b)

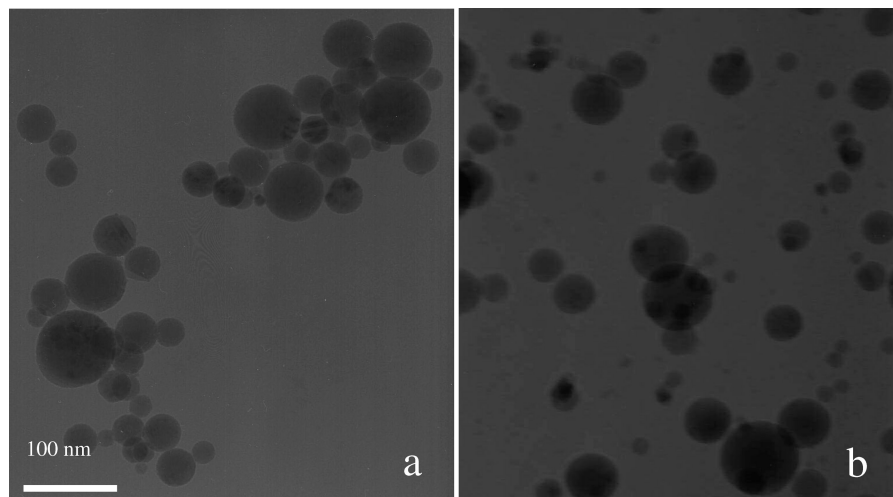


FIG. 1. Typical TEM image of iron oxide particles collected; 10 mm above the generation zone (a), from the nebulizer suspension (b).

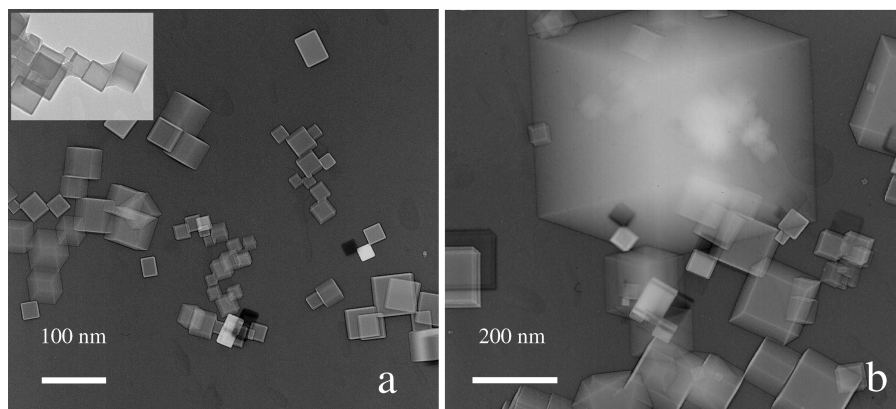


FIG. 2. TEM images of MgO particles collected at 10 mm above the flame. Non-agglomerated cubes are clearly distinguished in the wide range of sizes. For comparison, the insert in (a) shows agglomerated particles collected at 80 mm above the generation zone.

clearly demonstrates that all soft agglomerates likely appearing due to magnetic attraction of particles (see Figure 1a) were effectively broken and the vast majority of particles presented in the nebulizer are single.

Magnesium oxide nanoparticles, used in this research, represent the second group of nanoparticles, these being of cubic form. These particles (density 3.6 g/m^3) have a perfect cubic shape and their production (Altman, Agranovski, and Choi 2004) is very similar to the one described above for the iron oxide nanoparticles. TEM images of cubic magnesium oxide particles shown in Figure 2 clearly demonstrate that MgO cubes are non-agglomerated in the wide range of sizes up to 400 nm (see particle of corresponding size in Figure 2b). Also, as was shown in our recent publication (Altman, Agranovski, and Choi 2005), particles collected at the low height above the generation zone are not agglomerated, whilst collection at higher altitude could be associated with sintered clumps. For comparison, we show such sintered clumps collected at the height of 8 cm above the generation zone (see insert in Figure 2a). During combustion of the Mg particle, the MgO nanoparticles were collected on the substrate from the stream 10 mm above the flame, then brushed into the nanopure deionized water and their suspension was sonicated for, at least, 60 minutes before aerosolizing by the nebulizer.

Experimental Apparatus

Figure 3 shows the schematics of the experimental setup. Before reaching the nebulizer, the air was passed through three HEPA filters located in series to remove all extraneous aerosols entering the system and thus to ensure clean incoming air. The particle suspension (either PSL, magnesium oxide, or iron oxide), prepared as described above, was placed into the nebulizer (Model 8035, API, USA) and aerosolized to provide the test aerosol. After passing through the generator, the air was mixed in the mixing tube (diameter 15 mm and length 30 cm) with another portion of the dry HEPA filtered air to create condi-

tions for effective drying of moisture from the particle surface. The aerosol was then collected isokinetically through the intake pipe located at the distance of 20 cm from the mixing tube inlet (the distance has been chosen to provide complete mixing of air and particle streams). The aerosol was then passed through an electrostatic charge neutralizer (10-mCi ^{85}Kr , model 3012, TSI Inc., St. Paul, MN) used to neutralize particles before their entry to the DMA column. Alternatively, to flush the system before each experiment, the aerosol intake line was shut down and the HEPA filtered air pipeline to the neutralizer was opened by two valves installed on the corresponding lines, as shown in the Figure 3. The DMA column (Model 3080, TSI

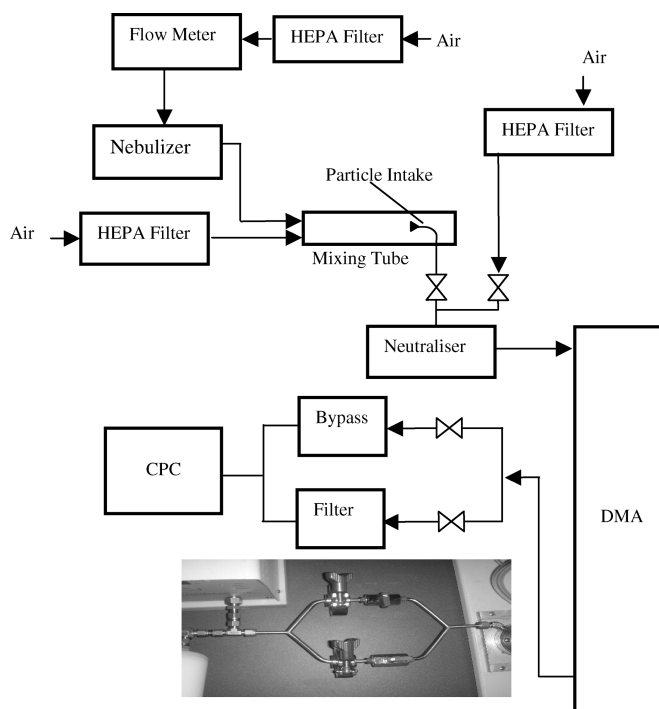


FIG. 3. Experimental apparatus.

Inc., St. Paul, MN) was used to prepare monodisperse particles of the required size for subsequent passage through the filter. The Condensation Particle Counter (CPC) (Model 3010, TSI Inc., St. Paul, MN) was used to measure particle concentration. Instead of the standard piping, commonly used for connection of DMA and CPC, a special filter holder has been made (see insert in Figure 3) to substitute for such piping. The holder consists of two identical parallel lines equipped with the hermetically sealed filter supports; one held a filter whilst the other was empty and served as the bypass line. The air stream could be directed to either one of them by valves located on both lines. Such an arrangement was convenient for obtaining the results for calculation of the filter efficiency without the necessity of frequent assembling/disassembling of the filter supports. The number of particles after passing through the filter represented the downstream concentration, whilst counting of particles after bypass line corresponded to the initial (upstream) concentration of aerosols. All flow rates were monitored and controlled by the flowmeters equipped with the adjusting valves.

Experimental Procedure

A fresh, 2 mm thick, polypropylene filter with the packing density of 9% and fiber size of 19 μm was secured in the holder and the valves were positioned to close the air access through the filter line and open it through the bypass line. The valves on the particle intake assembly were positioned to allow access through the HEPA filter and the device was operated until no particles remained in the system. After that, the valves were repositioned to open the particle intake line (keeping the HEPA filter line shut down) and the PSL particles of the selected size (out of 5 sizes mentioned above) were aerosolized by the generator, fed to the DMA column and their size distribution was obtained by the CPC. The magnitude of voltage representing the pick concentration (this voltage usually closely coincided with the corresponding particle size as given by the instrument) was recorded and the DMA column was turned to the monodisperse particle production regime when only one voltage was used during the entire procedure. The initial particle concentration in the bypass line was obtained and the valves were then switched to allow aerosol to pass through the filter while the bypass line was securely closed. The system was then flushed through the HEPA filters located at the entrance to the neutralizer until no particles remained in the system. Then, the experimental aerosols were fed back to the DMA and the particle count representing a number of particles penetrating through the filter was recorded. The filter efficiency was then calculated according to the classic equation (Brown 1993).

$$E_T = \left(1 - \frac{C_A}{C_B}\right) \times 100\% \quad [1]$$

where C_A and C_B are concentrations of the particles after passing through the filter line and the bypass line, respectively.

The filtration velocity of 0.02 m/s was used for all experimental runs. This velocity was chosen to fully exclude any influence of the inertial mechanism of filtration for the whole range of particle sizes of interest. Note that for 300 nm particles, and considering the substantial difference in their densities, the inertial mechanism could start to be influential at higher filtration velocities, and thus not permitting any direct comparison of the results.

The PSL spheres were monodisperse, while all other particles were initially polydisperse. The polydisperse aerosol provided by the nebulizer/generator, was passed through the DMA column at the voltage corresponding to the particular size of PSL spheres used in experiments to separate nanooxide particles of the equivalent size out of the sizes available in the mixture. Knowing the exact size of PSL particles, we were able to accurately control the voltage applied to the DMA, which corresponds to the particle of the same mobility as the PSL particles. Then the monodisperse aerosol was passed through the filter/bypass lines to obtain C_A and C_B for the subsequent efficiency calculations, as outlined above. The same procedure was used to obtain the results for five sizes for all three types of nanoparticles.

It is important to highlight that, to avoid the influence of the previously captured particles on the filtration efficiency, a fresh filter was used for each experimental measurement. Also, at least five experimental repeats were undertaken for each particle size to obtain reliable results.

RESULTS AND DISCUSSION

Figure 4 shows the overall original particle size distribution of iron and magnesium oxide particles used in the experiment, as measured by SMPS. As is seen, both substances demonstrate reasonably similar trends with the peak at around 35 nm. For the experimental runs, particles of a selected size were separated by

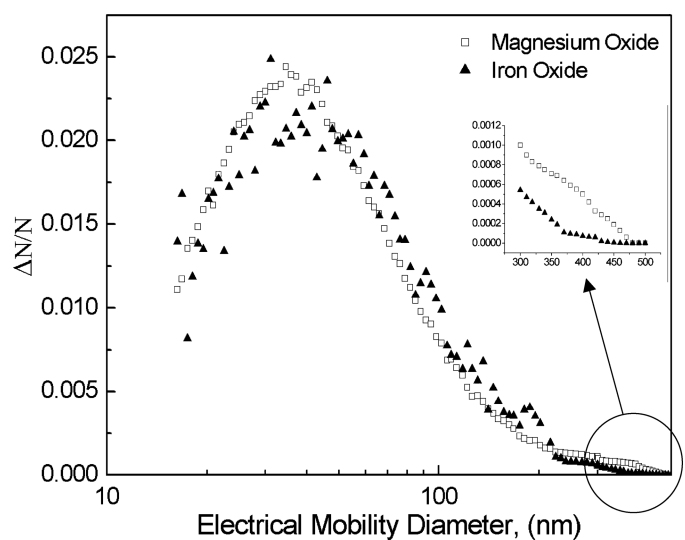


FIG. 4. Size distribution of magnesium and iron oxide particles measured with SMPS.

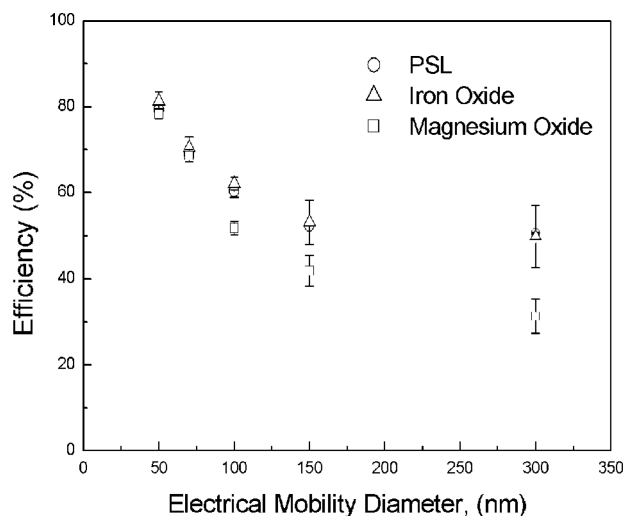


FIG. 5. Measured filter efficiency for cubes and spheres.

the DMA from the polydisperse aerosol and passed to the fibrous filter stage. To obtain a representative number of particles of each size used in experiments, the amount of dry nanooxide powder added to the water in the nebulizer was adjusted. In general, for particles within the range of 50–150 nm, the number of particles was of the order of $5 \times 10^4 \text{ cm}^{-3}$ for both nanooxides. For the largest particle size of 300 nm, considering their weak contribution to the general size distribution, the maximum number of particles which we managed to achieve, was around 3000 cm^{-3} . However, considering a very high consistency of the results (discrepancy between similar experimental runs did not exceed 4% of measured quantity), these numbers of particles was decided to be satisfactory.

Figure 5 shows the filter efficiency for all particles investigated. The error bars represent the standard deviation of, at least, 5 experimental runs. The efficiency is plotted vs. the particle mobility diameter for all experiments which were performed at the velocity of 0.02 m/s at the filter face. Two main conclusions can be summarized, namely

1. The filtration efficiency of nanoparticles within the studied size region and for the chosen air velocity does not depend on the particle density. This conclusion is fully supported by the efficiency curves for spherical PSL and iron oxide fully coinciding along the whole range of sizes investigated.
2. The filtration efficiency of cubic particles is lower than that of spherical particles. It is clearly observed that the efficiency difference for bigger particles is much larger compared to that for the small ones within the investigated range of diameters.

Simple consideration could be undertaken to analyze the process of nanoparticle filtration. As is well known, different mechanisms contribute to the particle filtration efficiency. They are (Hinds 1999) interception, inertial impaction, diffusion, gravitational settling and electrostatic attraction. Substituting our

particular process parameters into the equations derived for each filtration mechanism shows that:

1. The interception does not play a crucial role due to the fact that the average ratio of a particle size to a fiber diameter is 1:200 which corresponds to a very low contribution of interception to the total single fiber efficiency (even for largest particles, the interception efficiency is $\sim 4 \times 10^{-4}$).
2. Considering the very small particle size and low filtration velocity used in the experiments, the inertial impaction also does not contribute much towards the enhancement of filtration efficiency. Its maximum value is around 2×10^{-7} for particles of 300 nm diameter.
3. Electrostatic attraction could also be excluded from consideration as most of particles coming from the DMA column have a unit charge and would behave similarly regardless of their shapes. Also, the influence of some possible fiber charging could be neglected, as experimental conditions were the same for all particle types.
4. Some possible double charging of 300 nm particles may occur. Hinds (1999) notes that $\sim 9\%$ of particles of that size could be double charged. This could make a corresponding contribution towards the counting of 150 nm particles. This effect may be eliminated from consideration, as it could occur with all types of particles with similar equivalent diameter. There is the related possibility of the existence of double charged 600 nm particles with their corresponding contribution to the 300 nm particle count. Careful observation of more than 100 TEM photographs of each of the nanooxides, shows that the largest particle found across all of them was 493 nm. Of course, such a finding does not mean that larger particles do not exist at all, however, their number is negligibly small and can not contribute significantly toward the current results. Also, an excellent agreement between the results obtained for monodisperse PSL particles and iron oxide spheres, strongly supports the exclusion of double charging from consideration.
5. Obviously, due to the very small particle size, gravitational settlement is also excluded from consideration

Finally, according to the classic theory of filtration, diffusion is a dominant process for small particle filtration. The filtration efficiency of diffusion is proportional to the Peclet number (Hinds 1999), that is, to the particle mobility. As the same particle mobility mechanism is responsible for aerosol separation in the DMA column, the filtration efficiency of spherical particles of the same size (the same mobility), even of different densities, is not surprising. Applying a similar approach would imply that the filtration efficiency due to diffusion of magnesium oxide cubes should be the same as that for spheres. Indeed, the cubes having the same mobility do not differ from spheres if diffusion is considered. However, the significant difference between filtration efficiency of spheres and cubes is evidence that some effect (besides diffusion) becomes significant in the case

of cubic particles. It is obvious that this effect does not exist whilst the particle remains airborne and appears only after the particle-fiber collision event, and results from the different nature of the possible motion of spheres and cubes along the fiber surface. As we pointed out in the introduction, the spheres may slide and/or roll, whilst cubes would slide or tumble until being fully adhered (captured by a fiber) or rebounded (not captured). During the sphere sliding (or rolling) along the fiber, the contact area is not changed. Then, it may be assumed that this motion could not affect the bounce probability, and correspondingly, no difference between the spherical particles of different densities was observed in the experiments. A totally different process occurs in the case of the motion of the cube, when due to the tumbling, the face alignment of a cube may not be achieved before the particle is pulled off the surface. This disables the cube adhering causing its rebounding; the particle could be easily detached at the moment when it contacts the fiber via the edge.

The measured filter efficiencies for spheres and cubes allow us to evaluate the probability of additional, compared to spherical particles, rebound of cubes. The overall filter efficiency measured in the experiment can be expressed as (Brown 1993):

$$\varepsilon_{\text{exp}} = 1 - \exp(-k_f \varepsilon_0), \quad [2]$$

where ε_0 is the single fiber efficiency. The coefficient k_f represents the physical parameters of the filter (fiber size, packing density, and thickness) and does not depend on the properties of the filtered particles.

Simple analysis of Equation 2 shows that the filter efficiency for the cubes could be lower than that for the spheres due to some additional possibility of bouncing, as all other process parameters and, correspondingly, magnitudes of filtration mechanisms are theoretically identical for both cases. This additional rebound probability, p , contributes to the single fiber efficiency and can, respectively, be written as

$$\varepsilon_0^{\text{cubes}} = (1 - p) \varepsilon_0^{\text{spheres}}, \quad [3]$$

where $\varepsilon_0^{\text{cubes}}$ and $\varepsilon_0^{\text{spheres}}$ are the single fiber efficiencies for cubes and spheres. Combining Equations (2) and (3) yields

$$p = \frac{\ln(1 - \varepsilon_{\text{exp}}^{\text{spheres}}) - \ln(1 - \varepsilon_{\text{exp}}^{\text{cubes}})}{\ln(1 - \varepsilon_{\text{exp}}^{\text{spheres}})}, \quad [4]$$

where $\varepsilon_{\text{exp}}^{\text{cubes}}$ and $\varepsilon_{\text{exp}}^{\text{spheres}}$ are the overall filter efficiencies measured for cubes and spheres in experiments described above.

Obviously, the particle tumbling is a kinetic process, which may be associated with the particle kinetic energy ($mV^2/2$) characterizing the particle motion in the flow, where m represents the particle mass and V is the filtration velocity. On this basis, the kinetic energy could be suggested as a parameter describing an efficiency of the particle re-entrainment during its tumbling.

TABLE 1

Kinetic energy of different size magnesium oxide particles at flow velocity of $V = 0.02$ m/s

Particle size (nm)	Kinetic Energy (meV)
50	0.3
70	0.8
100	2.4
150	8
300	64

Table 1 shows the magnitude of the kinetic energy calculated for all sizes of magnesium oxide particles involved in this investigation. Clearly, the kinetic energy is rising with the increase of the particle size. Correspondingly, in the experiment, the increase of this parameter is accompanied by the increase of the deviation between the filtration efficiency of spherical and cubic particles. On this basis, the energy could realistically characterize the efficiency of the shaped particle re-entrainment during filtration and, therefore, it may be used to describe the additional bounce probability appearing in the case of the filtration of cubic particles.

Figure 6 shows the results for p as derived from the experimental data according to the procedure described above. The probability of additional bouncing, p , is plotted versus the particle kinetic energy. The dashed line is a guide for the eye. It is obtained by fitting the function of energy E

$$p(E) = A - B \exp\left(-\frac{E}{C}\right) \quad [5]$$

to the data. Fitting parameters corresponding to the dashed line in Figure 6 are as follows: $A = 0.453$, $B = 0.437$, $C = 7.19$ meV.

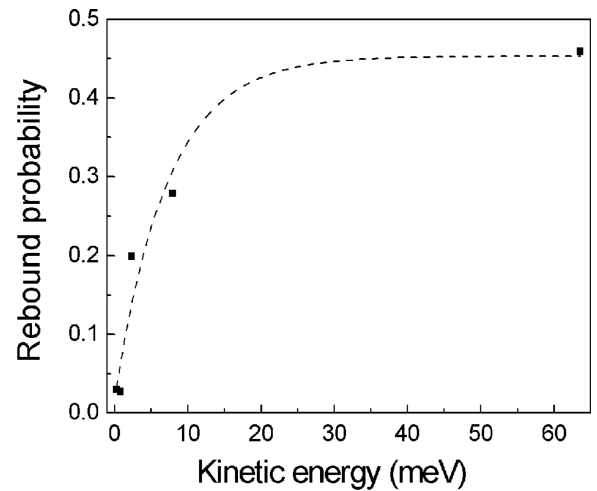


FIG. 6. Additional rebound probability of cubic particles.

CONCLUSION

It has been shown that the variation in particle density does not affect the removal efficiency of the spherical nanoparticles even if their densities vary by a factor of five.

It is evident from our work that the filtration efficiency is significantly different for cubic and spherical nanoparticles and that this deviation in efficiency is increasing with increase of the particle size in the range 50 nm to 300 nm. After excluding the diffusion mechanism as a possible factor responsible for such a difference, it was concluded that its main cause is likely to be the nature of motion of cubes and spheres along the fiber surface; the spherical particles could either slide or roll whilst the cubic ones slide or tumble. Following this consideration, the parameter (kinetic energy) describing the contribution of the particle tumbling toward the filtration efficiency was proposed and quantified. It is clearly shown that tumbling plays a significant role in the process of filtration of non-spherical nanoparticle on fibrous filters.

This work represents the first step to describe a very complicated process. Further research will be undertaken to deeper understand various mechanisms of interaction between complex-shape nanoparticle and fiber and to determine and quantify in detail the exact cause of this behavior.

REFERENCES

- Altman, I. S., Agranovski, I. E., and Choi, M. (2004). On Nanoparticle Surface Growth: MgO Nanoparticle Formation During a Mg Particle Combustion, *Appl. Phys. Lett.* 84:5130–5132.
- Altman, I. S., Jang, Y.-H., Agranovski, I. E., Yang, S., and Choi, M. (2004). Stabilization of Spinel Structure During Combustion Synthesis of Iron Nanooxides, *J. Nanoparticle Res.* 6:633–637.
- Altman, I. S., Agranovski, I. E., and Choi, M. (2005). Mechanism of Nanoparticle Agglomeration During the Combustion Synthesis, *Appl. Phys. Lett.* 87:053104.
- Bradley, R. S. (1932). The Cohesive Force Between Solid Surfaces and the Surface Energy of Solids, *Phil. Mag.* 13:853–862.
- Brown, R. C. (1993). *Air Filtration: An Integrated Approach to the Theory and Applications of Fibrous Filters*. Pergamon Press, Oxford.
- Dahneke, B. (1971). The Capture of Aerosol Particles by Surfaces, *J. Coll. Interface Sci.* 37:342–353.
- Dahneke, B. (1973). Measurements of the Bouncing of Small Latex Spheres, *J. Coll. Interface Sci.* 45(3):584–590.
- Dahneke, B. (1975). Further Measurements of the Bouncing of Small Latex Spheres, *J. Coll. Interface Sci.* 51(1):58–65.
- Dahneke, B. (1995). Particle Bounce or Capture—Search for an Adequate Theory: I Conservation-of-Energy Model for a Simple Collision Process, *Aerosol Sci. Technol.* 23:25–39.
- Deryaguin, B. V., Muller, V. M., Mikhovich, N. S., and Toporov, Y. P. (1987). Influence of Contact Electrification on the Collision of Elastic Particles with a Rigid Surface, *J. Coll. Interface Sci.* 118(2):553–563.
- Gallily, I., and La Mer, V. K. (1958). On the Behavior of Liquid Droplets After Impinging on Solid Surfaces, *J. Phys. Chem.* 62:1295.
- Gillespie, T., and Rideal, E. (1955). On the Adhesion of Drops and Particles on Impact at Solid Surfaces, *J. Col. Sci.* 10:281–298.
- Hamaker, H. C. (1937). The London-Van der Waals Attraction Between Spherical Particles, *Physica* 4:1058–1072.
- Hinds, W. C. (1999). *Aerosol Technology: Properties, Behavior, and Measurement of Airborne Particles*, John Wiley and Sons, New York.
- Johnson, K., Kendall, K., and Roberts, A. D. (1971). Surface Energy and the Contact of Elastic Solids, *Proc. R. Soc. Lond. A.* 324:301–313.
- Loeffler, F. (1971). Blow-off of particles collected on filter fibers. *Filtration Society Conf. London:* 28–30.
- Loeffler, F. (1974). Adhesion Probability in Fibre Filters, *Clean Air* 8(4):75–78.
- Mullins, B. J., Agranovski, I. E., and Braddock, R. D. (2003). Particle Bounce During Filtration of Particles on Wet and Dry Filters, *Aerosol Sci. Technol.* 37:1–14.
- Mullins, M. E., Michaels, L. P., Menon, V., Locke, B., and Ranade, M. B. (1992). Effect of Geometry on Particle Adhesion, *Aerosol Sci. Technol.* 17:105–118.
- Rimai, D. S., Demejo, L. P., and Bowen, R. C. (1994). Mechanics of Particle Adhesion, *J. Adhesion Sci. Technol.* 8(11):1333–1355.
- Stenhouse, J. I. (1972). The Behaviour (to check) of Fibrous Filters in High Inertia Systems, *Proc. Filtration Soc. in Filtration and Separation:*426–428.
- Tsai, C.-J., Pui, D. Y. H., and Liu, B. Y. H. (1991). Elastic Flattening and Particle Adhesion, *Aerosol Sci. Technol.* 15:293–255.
- Wall, S., John, W., Wang, H.-C., and Goren, S. (1990). Measurements of Kinetic Energy Loss for Particles Impacting Surfaces, *Aerosol Sci. Technol.* 12:926–946.
- Wang, H.-C., and Kasper, G. (1991). Filtration Efficiency on Nanometer-Size Aerosol Particles, *J. Aerosol Sci.* 22:31–41.
- Wang, H.-C., and John, W. (1987). Comparative Bounce Properties of Particle Materials, *Aerosol Sci. Technol.* 7(3):285–299.
- Xu, M., and Willeke, K. (1993). Technique Development for Particle Bounce Monitoring of Unknown Aerosol Particles, *Aerosol Sci. Technol.* 18:129–142.